Article

Methods

A model of functionally buffered deleterious mutations can lead to signatures of positive selection distinguishable from an evolutionary conflict model

Runxi Shen[†1], Miwa Wenzel[†2], Philipp W. Messer[1], Charles F. Aquadro[2]

[1] Department of Computational Biology, Cornell University, Ithaca, NY, USA

[2] Department of Molecular Biology and Genetics, Cornell University, Ithaca, NY, USA

[†] These authors contributed equally to this work.

*Corresponding author: Email: cfa1@cornell.edu

Abstract

Selective pressures on DNA sequences often result in signatures of departures from neutral evolution that can be captured by the McDonald-Kreitman (MK) test. However, the nature of such selective forces mostly remains unknown to the experimentalists. Here we use the *bag of marbles* (*bam*) gene in *Drosophila* to investigate different types of driving forces behind positive selection. We examine two evolutionary models for *bam.* The Conflict model originates from a conflict of fitness between *Drosophila* and *Wolbachia* that causes reciprocal adaptations in each, resulting in diversifying selection on the *bam* protein. In the alternative Buffering model, *Wolbachia* protects *bam* from deleterious mutations during an infection and thereby allows such mutations to accumulate and even fix in the population. If *Wolbachia* is subsequently lost from the species, mutations that revert the gene back towards its original biological function become advantageous. We use simulations to show that both models produce signals of positive selection, though the levels of positive selection under the Conflict model are more easily detected by the MK test. By fitting the two models to the empirical divergence of *D. melanogaster* from an inferred ancestral sequence, we found that the Conflict model reproduced strong signals of positive selection like those observed empirically, while the Buffering model better recapitulated the physicochemical signatures of the amino acid sequence evolution at *bam.* Our demonstration that the Buffering model can lead to positive selection suggests a novel mechanism that needs to be considered behind observed signals of positive selection on protein coding genes.

Introduction

Patterns of DNA sequence variation within and between species have increasingly been used to infer the evolutionary forces that have acted on genes and genomes. Over the past three decades, many tests of fit to a model of neutral evolution have been developed, with one of the most widely applied being that proposed by McDonald and Kreitman (McDonald and Kreitman 1991) and referred to as the McDonald-Kreitman (MK) test. The basis of this test is a comparison of the ratios of nonsynonymous and synonymous fixed differences between species to those segregating as polymorphisms within species using a 2x2 contingency test (e.g., Fisher's Exact Test, Chi-Square test, or G-test). Synonymous variation acts as a proxy for neutral variation (or at least variation that does not directly alter the protein sequence of genes), with an

excess of nonsynonymous fixed differences between species typically interpreted as evidence that some form of natural selection has accelerated the fixation of advantageous amino acid replacements. This pattern is often referred to as positive selection and is interpreted to mean that natural selection has been fine tuning the protein function of the gene or responding to a changing function, and/or that the gene is involved with intra- or inter-genomic conflict (McLaughlin and Malik 2017). Although the MK test has been found previously to have low power to detect positive selection, particularly when applied to single genes (Akashi 1999; Zhai et al. 2009), there are many empirical reports in the literature of significant departures in the direction of positive selection (e.g., Eyre-Walker 2006). The obvious question from the experimentalist's perspective is what evolutionary mechanisms are driving such signatures of positive selection.

We have studied the population genetics of two *Drosophila* genes that are critical for gametogenesis in *D. melanogaster* (*bag of marbles, bam*, and *Sex-lethal, Sxl*) and they both show evidence, using the MK test, of episodic bursts of positive selection (Bauer DuMont et al. 2007; Flores et al. 2015a; Bauer DuMont et al. 2021). These genes genetically interact with the endosymbiont bacteria *Wolbachia pipientis* in that *Wolbachia* rescues the reduced fertility of a partial loss-of-function *bam* mutant and the reduced egg production of multiple partial loss-of-function *Sxl* mutants (Starr and Cline 2002; Flores et al. 2015b; Bubnell et al. 2021). The bursts of positive selection in *bam* in only certain lineages of *Drosophila* is consistent with the episodic nature of bacterial infections and the heterogeneous presence of *Wolbachia* reported across the genus (Richardson, et al. 2012; Turelli, et al. 2018; Meany, et al. 2019). These observations, along with the knowledge that functional divergence in *bam* is seen primarily in females, and that maternally-inherited *Wolbachia* physically resides in the germarium and manipulates reproduction of its host (Flores et al. 2015b) led Bauer DuMont et al. (2007), Flores et al. (2015a) and Flores et al. (2015b) to propose that evolutionary conflict between the host (*Drosophila melanogaster*) and *Wolbachia* over the control of reproduction may drive the observed positive selection at *bam*.

Here, we explore the dynamics of protein sequence evolution under two evolutionary models that we hypothesize could be responsible for the burst of positive selection we see at *bam.* The first is a classic arms race conflict model. In this model, we assume that *Wolbachia* infection is detrimental to a germline reproductive process in which *bam* is involved. For

example, *Wolbachia* may manipulate *bam* in a way counterproductive to the fitness of the fly. Under arms race dynamics, we would expect positive selection to favor diversifying amino acids in *bam* that result in *Drosophila's* escape from the deleterious impact of *Wolbachia* on their fitness. We term this the Conflict model. Note that while we model this as an evolutionary conflict, selection associated with a strong directional shift in function would be similar in outcome in many ways.

Secondly, we propose and evaluate a new model of interaction that is based on the nature of the observed genetic interactions of *Wolbachia* with *bam* and *Sxl*. *Wolbachia* partially rescues the fertility defects of a single amino acid replacement hypomorphic mutant of *bam* (Flores et al. 2015b, Bubnell et al. 2021) as well as for several hypomorphic alleles of *Sxl* (Starr and Cline 2002) in *D. melanogaster.* We posit that in the presence of *Wolbachia*, slightly deleterious mutations may accumulate in the *bam* gene without significantly reducing *bam's* function. When *Wolbachia* is lost from the population, there is positive selection for new nonsynonymous mutations that return the *bam* protein sequence to its initial, and assumed optimal, functional state. We term this model the Buffering model, as the effects of deleterious mutations are "buffered" during periods of infection by *Wolbachia*.

We carry out evolutionary simulations to explore the population genetic consequences for sequence evolution at *bam* for both conflict and buffering interactions between the endosymbiont *Wolbachia* and the *Drosophila* host. With these models, we first reaffirm the resultant adaptive evolution of a theoretical arms race conflict and assess the likelihood that the alternative buffering type of interaction can also result in signatures of positive selection detectable with the MK test. We then evaluate the robustness of these models to variation in selection coefficients and duration of *Wolbachia* infection, and test our ability to distinguish between the two models using a measure of amino acid similarity (Miyata et al. 1979). Finally, using model parameters tuned to the observed sequences of *bam* in *D. melanogaster*, we evaluate evidence from the observed sequence divergence of *bam* in *D. melanogaster* compared to its common ancestor with *D. simulans* to see if we can discriminate as to which model (Conflict or Buffering) better captures the signatures of the bursts of positive selection observed at *bam*.

Materials and Methods

Simulation setup using SLiM 3.5

The evolution of *bam* was simulated under a Wright-Fisher model using nucleotide-based simulation in SLiM 3.5 (Haller and Messer 2019; Haller et al. 2019). We inferred the ancestral DNA sequence of the exons in *bam* (1338 nucleotides) for *Drosophila melanogaster* and *Drosophila simulans* using maximum likelihood with codeML v4.8 (Yang 2007). Briefly, alignments of seven *Drosophila* coding sequences were made using PRANK v.170427 (Löytynoja 2014), including sequences of *D. melanogaster, D. simulans, D. sechellia, D. yakuba, D. erecta, D. eugracilis, and D. pseudoobscura*. The alignment was input in codeML and an ancestral sequence was estimated by maximum likelihood for the common ancestor of *D. melanogaster* and *D. simulans*, using the other species' sequences as outgroup references. The estimated common ancestral nucleotide sequence was then used in SLiM as the starting sequence for the entire population in each simulation.

The evolutionary parameters in the simulations were based on empirical estimates and then scaled to make the simulations run efficiently (summarized in Table 1). The reported evolutionary parameters from empirical observations were an effective population size (N_e) of 1e6 (Campos et al. 2017), an overall mutation probability (μ) of 2.8e-9 per nucleotide per generation (Keightley et al. 2014), an average recombination rate (ρ) of 1e-8 per nucleotide per generation (Comeron et al. 2012) and a divergence time t of 25 million generations (2.5 million years assuming 10 generations per year) from the common ancestor to each species (Russo et al. 1995). These parameters were then scaled down by 1,000 to run more efficient simulations by using a smaller population and shorter simulation time while keeping the key products, $N_e\mu$, $N_e r$ and N_e/t constant to approximate the same evolutionary process (Haller and Messer 2019). Hence, in each Wright-Fisher simulation, we have 1) a scaled population size N_e of 1,000 diploid individuals, 2) a mutation matrix representing a Kimura (1980) model with transition rate α and transversion rate β of 1.88e-6 and 0.47e-6 respectively (calculated from a scaled mutation rate μ=2.8e-6 and an observed 2:1 transition:transversion ratio in the sequences (Keightley et al. 2009)), 3) a scaled recombination rate ρ of 1e-5 and 4) 25,000 scaled generations for the divergence time t. We simulated *bam* as a single contiguous exon, though in reality there are two short introns (61 and 64 bp). The effect of excluding these introns had a negligible impact on the rate of recombination.

We observed 85% of the codons in *bam* encode the same amino acids in both *D. melanogaster* and *D. simulans* reference sequences, likely due to functional constraints (example

classifications are show in supplemental fig. S1). Thus, we used this metric as a baseline in our initial simulations and first randomly sampled 75% of the codons among the 1338 nucleotide sites from the identical amino acids in the ancestral sequence to be constrained to the original amino acids. The rest of the identical amino acids (10% of the total amino acids) were assumed to be under completely neutral evolution, while the other 15% unidentical amino acids were under selection based on the setup of our models. A nonsynonymous mutation in the conserved codons was always assigned a selection coefficient s = -0.1, so that it would undergo strong purifying selection ($N_e s$ = -100 in our simulations). Note that the fitness of an individual in SLiM is calculated multiplicatively as (1+s) when it carries a homozygous mutation of selection coefficient s and (1+hs) when the mutation is heterozygous, where h is the dominance coefficient. In all our simulations, the dominance coefficient of any mutation was set to a constant of 0.5. A mutation in the neutral codons was always assigned a selection coefficient s = 0.

Each simulation run began with a neutral "burn-in" period of 20,000 simulation generations (=20×scaled N_e) to accumulate genetic variation consistent with an equilibrium state of mutation-drift balance before non-neutral dynamics started. Note that during this neutral period, mutations occurring at the conserved sites were still assigned a selection coefficient of s = -0.1 to retain the functionally constrained amino acid positions. At the end of the neutral "burn-in" period all new variations (fixations and polymorphisms) were retained in the simulation. However, the "reference sequence" in SLiM that is used to track the substitutions in the population and to assign selection coefficients in the upcoming non-neutral phases of the simulation, was manually reset to the original estimated ancestral sequence inferred from PAML. We did this so the selection coefficients of subsequent new mutations would be based on the particular amino acid change encoded by the new mutation compared with the original inferred ancestral sequence.

For each selection phase of the simulations, the absolute value of selection coefficient $|s|$ for each positively or negatively selected mutation in the 15% of codon sites under selection was fixed for the duration of each simulation. The beneficial mutations were assigned a selection coefficient of $s > 0$ while deleterious mutations had a selection coefficient $s < 0$. To determine the fitness effect of each mutation, we explored several correlated measures of amino acid substitutions (e.g., Grantham et al. 1974; Miyata et al. 1979; Henikoff and Henikoff 1992). We

used the amino acid matrix of Miyata et al. (1979), which captures the primary features of biochemical and physical differences between amino acid pairs but does not take empirical protein sequence conservation into account, since some of our changes were going to be positively selected, and not conserved. We henceforth refer to the pairwise measures from the Miyata matrix as "Miyata scores (MS)" and use them to determine whether a mutation is neutral (synonymous, no change in the encoded amino acid) or under positive or negative selection (nonsynonymous, MS between the original amino acid and the mutated amino acid $\neq 0$) in each selection scenario. Below, we will use a shorthand for Miyata score calculations as follows, with, for example, MS between the current amino acid and the mutated amino acid represented as $MS(AA_{cur}, AA_{mut})$.

Selection regimes

Wolbachia infections have been observed to be temporally dynamic in host populations, being lost at times and then regained, even from another species of *Drosophila* (Richardson et al. 2012; Turelli et al. 2018; Meany et al. 2019). Thus, each model has two selection phases: one with selection parameters to represent a period of *Wolbachia* infection and another to represent a period of *Wolbachia* absence in the population. There are four different selection schemes: 1a) *Wolbachia*-infection phase in the Conflict model, 1b) *Wolbachia*-absence phase in the Conflict model, 2a) *Wolbachia*-infection phase in the Buffering model, and 2b) *Wolbachia*-absence phase in the Buffering model. The phases of infection and absence of *Wolbachia* alternated in each model, which simulated the periodic occurrence of *Wolbachia* in natural populations. To keep the simulations simple, we assume that *Wolbachia* infection and loss is instantaneous throughout the entire population and that there are no other effects of *Wolbachia* on the host beyond which we are modeling.

The Conflict model was implemented based on a traditional arms race model. In the *Wolbachia*-infection phase, we assume that *Wolbachia*'s presence drives the positive selection of *Drosophila* by favoring the nucleotide changes that lead to biochemically more diversified amino acids to "escape" the present function which may be targeted by *Wolbachia*'s harmful impact. In this case, all the nonsynonymous mutations that give rise to biochemically different amino acids from the current states ($MS(AA_{cur}, AA_{mut}) > 0$) were positively selected for, with selection coefficients $s > 0$ (fig. 1, top).

In the *Wolbachia*-absence phase of the Conflict model, there is no evolutionary conflict between *bam* and *Wolbachia* and thus no selective pressure on the host to adapt. Under these conditions, we assume that the current amino acid sequence functions adequately such that the DNA sequences in the population remain largely unchanged and the *bam* gene is under purifying selection to preserve the present amino acid sequences. In this case, nonsynonymous mutations leading to amino acid changes ($MS(AA_{cur}, AA_{mut}) > 0$) are considered deleterious with selection coefficients $s < 0$ (fig. 1, top).

The second evolutionary model, the Buffering model, is built on the observation that *Wolbachia* offers a functional buffer for deleterious mutations in *bam* and rescues what would be reduced fertility of its host in the absence of *Wolbachia*. During the *Wolbachia*-infection phase, *Wolbachia* somehow functionally alleviates the deleterious effects of certain nonsynonymous mutations and makes them effectively neutral. Under this scenario, mutations leading to divergent amino acids different from the ancestral state ($MS(AA_{anc}, AA_{mut}) > 0$) are all regarded as neutral (fig. 1, bottom) and thus can accumulate, albeit slowly due to drift alone. If *Wolbachia* infection is lost, these previously buffered mutations are now deleterious, and new mutations leading to amino acids that converge back towards the initial amino acid ancestral states are favored as there is selective pressure for *bam* to regain its original optimal function. In this case, a mutation that converts the current amino acid to a mutated amino acid that is biochemically more similar to the ancestral amino acid ($MS(AA_{anc}, AA_{mut}) - MS(AA_{anc}, AA_{cur}) < 0$) is beneficial with a selection coefficient $s > 0$, while divergent mutations ($MS(AA_{anc}, AA_{cur}) - MS(AA_{anc}, AA_{cur}) > 0$) are deleterious with selection coefficients $s < 0$ (fig. 1, bottom).

The above models capture two types of potential driving forces behind the signatures of positive selection observed on the *bam* gene. However, these models make many idealized assumptions about amino acid evolution based on Miyata scores and thus are regarded as the "Base" models. For instance, in the Conflict model, any nonsynonymous mutation would be positively selected during the presence of *Wolbachia*. However, mutations that lead to biochemically similar amino acids with homogeneous functions may not bear such strong selective advantages compared to the original ones and could be regarded as almost neutral, while the mutations giving rise to extremely dissimilar amino acids may completely lose their original functionality and thus be deleterious. To incorporate these more realistic biological assumptions, we set up additional "Complex" models based on empirical observations to

231 determine whether a mutation would be neutral, beneficial, or deleterious. For example,
232 Demogines et al. (2013) identified adaptively evolving sites in the transferrin receptor gene *TfR1*
233 in wild rodents to include amino acids R, K, N, I, and T, which corresponds with pairwise
234 Miyata scores ranging from 0.4 to 3.37. Likewise, Charron et al. (2008) propose sites in the plant
235 gene eIF4E to be in an arms race conflict with viral proteins, which includes those with amino
236 acids L, P, and A that give pairwise Miyata scores ranging from 0.06 to 2.76. We found that the
237 Miyata scores for all proposed positively selected residues in these studies ranged from 0.05 to
238 3.37, with the majority of scores falling between 1.5 and 2.5.
239 With the above proposition, in the complex Conflict model when *Wolbachia* is present,
240 nonsynonymous mutations that give rise to biochemically similar amino acids ($0 < MS(AA_{cur}$,
241 $AA_{mut}) \leq 1$) are regarded as neutral with selection coefficients $s = 0$ (fig. 2, top); mutations
242 leading to mildly different amino acids ($1 < MS(AA_{cur}, AA_{mut}) \leq 3$) are considered beneficial
243 with selection coefficients $s > 0$ (fig. 2, top); and mutations become deleterious with selection
244 coefficients $s < 0$ when they generate extremely dissimilar amino acids ($MS(AA_{cur}, AA_{mut}) > 3$)
245 (fig. 2, top), as they are likely to disrupt the biological function of *bam*. These cutoffs are
246 consistent with the range of Miyata scores found at sites that are proposed to be adaptively
247 evolving in response to an evolutionary conflict. In the *Wolbachia*-absence phase in the complex
248 Conflict model, to preserve the current amino acid sequences, we still assume that mutations
249 leading to similar amino acid changes ($0 < MS(AA_{cur}, AA_{mut}) \leq 1$) are considered neutral, but
250 any mutation that causes a dissimilar amino acid change ($MS(AA_{cur}, AA_{mut}) > 1$) is deleterious
251 with a selection coefficient $s < 0$ (fig. 2, top).
252 Unlike the complex Conflict model, we have insufficient empirical observations to guide
253 our selection cutoffs for a complex Buffering model. For simplicity, we adopted the same
254 selection schemes used in the complex Conflict model to represent one biologically plausible
255 possibility for the interaction. When *Wolbachia* is infecting in the complex Buffering model, any
256 mutation that gives rise to a mildly biochemically different amino acid from the ancestral state (0
257 $< MS(AA_{anc}, AA_{mut}) \leq 3$) is regarded as neutral with selection coefficients $s = 0$ (fig. 2, below)
258 due to the protection by *Wolbachia*. However, mutations are considered deleterious with
259 selection coefficients $s < 0$ when they generate extremely dissimilar amino acids ($MS(AA_{anc}$,
260 $AA_{mut}) > 3$) (fig. 2, bottom), since they are likely to disrupt the biological function of *bam*.
261 When *Wolbachia* is lost from the population, only mutations that converge back towards the

biochemical characteristics of the initial ancestral state relative to the current amino acid are favored ($MS(AA_{anc}, AA_{mut}) - MS(AA_{anc}, AA_{mut}) < -1$) with a selection coefficient $s > 0$, while the more divergent mutations ($MS(AA_{anc}, AA_{mut}) - MS(AA_{anc}, AA_{cur}) > 1$) are deleterious with a selection coefficient $s < 0$ (fig. 2, bottom). Any mutation in between ($-1 \leq MS(AA_{anc}, AA_{mut}) - MS(AA_{anc}, AA_{cur}) \leq 1$) is considered neutral ($s = 0$) since it does not cause a radical functional change in the amino acid to increase or decrease the fitness of an individual. Below, we test the evolution of *bam* under both the "base" and "complex" models to investigate how implementation of different fitness parameterizations for the base and the complex Miyata score ranges affect our simulation results.

Simulation parameters

We focused on investigating the impacts of two key parameters on the evolution of the *Drosophila* species in each of the proposed models: 1) the magnitude of the selection coefficient for both beneficial and deleterious mutations, and 2) the length of alternating *Wolbachia*-infection and *Wolbachia*-absence phases in each model in which the different selection phases occur. The absolute values of selection coefficients included $|s| = 0.1$, $|s| = 0.01$, and $|s| = 0.001$, resulting in $N_e|s| = 100$, $N_e|s| = 10$, and $N_e|s| = 1$ respectively, where $N_e|s| = 1$ can be considered effectively neutral. The lengths of different selection phases varied from equal periods of 12,500, 6,250, and 3,125 simulation generations (corresponding to one, two, and four *Wolbachia* infection-loss cycle(s) respectively in a total divergence time of 25,000 simulation generations). For each set of parameter combinations, we ran 50 independent simulations and performed downstream analyses including the MK test, inferences of α (the proportion of amino acid fixations driven by positive selection; Smith and Eyre-Walker 2002), and Miyata score differences between the ancestral and evolved sequences. All these downstream analyses were conducted every 3,125 simulation generations (the shortest phase length in our simulation setup) after the neutral burn-in period, by comparing the "reference sequence" in SLiM to the common ancestral sequence of *D. melanogaster* and *D. simulans*. For the MK test, 100 diploid individuals were randomly sampled from the population and nonsynonymous and synonymous fixations (relative to the inferred ancestral sequence) and polymorphisms present were tabulated.

Analyses of simulated sequences

The MK test was used to evaluate departures from an equilibrium neutral model consistent with positive selection and was implemented with a custom script modified from the iMKT package (Murga-Moreno et al. 2019) to include mutations at 2-fold degenerate sites which the standard iMKT package implementation ignores. Polymorphisms and divergences found at 4-fold degenerate sites were considered synonymous and those found at 0-fold degenerate sites were considered nonsynonymous. If there was a polymorphism or divergence at a 2-fold site, the site was classified based on the synonymous or nonsynonymous nature of the resultant amino acid. Any sites in codons with a change at more than one position were rare in our simulations and ignored. The Fay et al. (2001) correction for low frequency polymorphisms was applied, counting only polymorphisms > 5% frequency to avoid including deleterious variation segregating in the populations. Significance of the MK test was determined by Fisher's exact test. An estimate of the proportion of amino acid causing nonsynonymous substitutions driven to fixation by positive selection ($\alpha = 1 - \frac{D_S P_n}{D_n P_S}$) was calculated from the input values of the MK test following Smith and Eyre-Walker (2002). We also calculated the "true α" in the simulations by tracking the actual fraction of nonsynonymous substitutions in *bam* that were driven to fixation by positive selection in the simulation. Since the selection coefficient of a mutation could change as *Wolbachia* was gained and lost from the population, any mutation that once had a selection coefficient $s > 0$ and was eventually fixed in the population was regarded as being driven to fixation by positive selection. As with the estimated iMKT α, the true α is calculated for each simulation from the observed substitutions relative to the ancestral sequence. The average Miyata score calculated for each amino acid change between the simulated, evolved sequence and the ancestral sequence was used as an assessment of physicochemical similarity between the two sequences.

Results

Conflict and Buffering Base Models

We first used the Conflict and Buffering Base models described above to simulate the cyclic pattern of *Wolbachia* infection and loss in the *Drosophila* population. In the Conflict Base model, nonsynonymous mutations underwent positive selection in the presence of *Wolbachia* infection but were negatively selected in the absence of *Wolbachia*. In the Buffering Base model,

nonsynonymous mutations experienced neutral evolution in the *Wolbachia*-infection phase but were positively or negatively selected in the *Wolbachia*-absence phase.

The patterns of true α's were clearly indicative of positive selection in the Conflict Base model phase with *Wolbachia* with the strongest selection ($N_e|s|$>100, fig. 3A, row 1). The elevated true α's persisted though with a slow decline during the subsequent Wolbachia-free phase. The Buffering Base model showed a positive, though much lower, α that emerges in the first *Wobachia*-absence phase (fig 3B, row 1), consistent with our intuition of positive selection to return to a more functional *bam* protein without the deleterious mutation buffering by *Wolbachia.* This pattern was also most evident with strong selection. Among all the selection coefficients for both the Conflict model and Buffering model, the true α's stayed high or increased in the phases where positive selection is expected and stayed constant or decreased in the phases of neutral evolution and purifying selection.

In the Conflict Base model, the average of iMKT estimates of α were almost all positive for selection coefficients with $N_e|s|$>1 and showed clear periodic changes as *Wolbachia* comes in and out of the population across all three phase lengths (fig. 3A, row 2). Surprisingly, the magnitude of the iMKT α's increased in the phase without the imposed positive selection. This unexpected increase is explained by the change of nonsynonymous polymorphisms (P_n) in the population. In the *Wolbachia*-infection phase, both D_n and P_n accumulated due to the positive selection of nonsynonymous mutations, as expected; however, after the sudden change to the *Wolbachia*-absence phase, D_n was largely unchanged while P_n experienced a sudden decrease as nonsynonymous mutations were all selected against (fig 3A, row 4). Given the equation for calculating the iMKT α ($\alpha = 1 - \frac{D_S P_n}{D_n P_S}$), the iMKT estimate of α therefore increased in the phase with the implemented purifying selection that followed the positive selection. For the effectively neutral case of $N_e|s| = 1$, the iMKT $\alpha's$ in the Conflict Base model fluctuated around 0.

In the Buffering Base model across all selection coefficients, the iMKT α's were mostly negative across the whole simulation, but changes in magnitude are evident in different selection phases, e.g., iMKT α decreased during neutral phases (*Wolbachia* present) but increased in phases with selection (*Wolbachia* absent) (fig. 3B, row 2). These observed negative iMKT estimates of α were due to the contributions from both D_n and P_n. In the initial *Wolbachia*-infection phase of the Buffering model, nonsynonymous polymorphisms were negatively selected in the constrained codons and neutrally buffered by *Wolbachia* in the codons under

selection, with few such mutations in the latter category going to fixation, explaining the negative iMKT α's in the initial phases (fig 3B, row 4). Following this "buffering" period, a subset of nonsynonymous mutations was selected for. However, the number of nonsynonymous mutations that could be positively selected in the Buffering Base model was much less than those in the Conflict Base model, leading to a smaller D_n and thus a smaller (possibly < 0) iMKT α, even when positive selection was present. While a periodicity of iMKT estimated α's was observed in both models, the small number of polymorphisms and fixed differences made these estimates only vaguely reflective of the true α's.

The boxplots of differences between the true and iMKT α's were used to evaluate the accuracy of iMKT α's. In general, iMKT α's systematically underestimate the true α's due to the presence of deleterious polymorphisms (Fay et al. 2001, Eyre-Walker and Keightley 2009, Messer and Petrov 2013). For the Conflict Base model with effectively neutral evolution ($N_e|s|$=1), iMKT α's usually underestimated the true α's (fig 3A, row 3). However, under stronger selection ($N_e|s|$=10 or 100), iMKT α's underestimated the true α's only during the *Wolbachia*-infection phase; there was good accuracy in iMKT α's estimation when *Wolbachia* was lost, which reflected the delay in detecting selection based on changing P_n as previously explained. In the Buffering Base model, iMKT α's also tended to underestimate the true α's (especially with $N_e|s|$>1 in the later *Wolbachia*-infection phases), with the boxplots distributed above 0.

For the Conflict Base model, the pattern of the true α's and the iMKT α's was not dramatically influenced by the magnitude of the selection coefficient ($N_e|s|$=10 or 100) and the varying lengths of the infection/absence periods that we examined. In contrast, for the Buffering Base model, longer *Wolbachia* infection periods resulted in larger true α's, presumably due to the greater time to accumulate buffered deleterious mutations in the presence of *Wolbachia*. Nevertheless, the length of *Wolbachia* infection and absence periods had only a minor impact on the final magnitude of D_n, D_s, P_n, and P_s observed at the end of the simulations (fig. 3A&B, row 4). Only P_n show dramatic periodic fluctuations due to the cyclic infection and absence periods.

Additionally, we looked at the distributions of p-values in iMKT (FWW correction, SNPs frequency > 5%) and the correlation between iMKT α's and their corresponding p-values at the end of the simulation. In general, a statistically significant rejection of neutrality in the direction of positive selection was more likely to be detected with the iMKT in the Conflict Base model

than in the Buffering Base model with the iMKT, since the values of the key MK test parameter D_n are generally much larger in both *Wolbachia*-infection and *Wolbachia*-absence phases in the Conflict model. This increased magnitude of D_n provided more statistical power in Fisher's exact test (fig. 5A). On the other hand, even under the strongest selection in our simulations, the MK test could hardly detect any statistically significant signals of positive selection in the Buffering model, likely due in part to the modest length of the *bam* gene (fig 5B). Overall, smaller p-values were always associated with larger iMKT α's, and all the significant p-values (<0.05) were associated with iMKT α's close to 1.0 across all selection coefficients (data not shown).

All together, these results demonstrated that α estimated from iMKT identified departures from neutrality in the direction of positive selection in the Conflict Base model but not reliably in the Buffering Base model. The phase without imposed positive selection in the Conflict model introduced a cyclical pattern of the iMKT α (but not the true α). The iMKT α was basically unreliable in all phases of the Buffering model. Lastly, the MK test parameter D_n reached a higher magnitude in the Conflict model, which was reflected in the smaller p-value statistics, suggesting greater power to detect positive selection with the MK test in the Conflict model than in the Buffering model.

Conflict and Buffering Complex Models

We next implemented the models with a more complex parameterization of selection coefficients based on Miyata scores. The MK test results for these Conflict and Buffering Complex models closely resembled those for the Base models. Since we narrowed down the Miyata score range for the positively selected nonsynonymous mutations in both complex models by introducing neutral and deleterious ranges, we observed lower true α's for both the Conflict and Buffering Complex models compared to their Base models (fig 4A&B, row 1). For the Buffering Complex model, this difference was particularly pronounced, with a barely perceptible increase in true α for even the strongest selection scenario of $N_e|s| = 100$. The patterns of iMKT α's and boxplots for the difference between the true and iMKT α's were similar between Complex and Base models (fig 4A&B, row 2&3). The total number of D_n did not reach the same magnitude at the end of simulation for the Conflict Complex model as it did in Conflict Base model across different phase lengths and selection coefficients. However, D_n had a slight increase in the Buffering Complex model compared with the Buffering Base model,

potentially due to the introduction of the neutral region leading to a small number of additional nonsynonymous fixations by genetic drift alone (fig 4A&B, row 4). The distributions of p-values were also similar between the Complex and Base cases (fig 5, C & D).

Distributions of Miyata scores

We expect amino acid substitutions to be more diversified in the Conflict model than in the Buffering model in both the Base and Complex cases, as the former is based on the premise of a sequence evolving *away* from the ancestral sequence and the latter is based on the premise of a sequence evolving *toward* the ancestral sequence. To assess this, we calculated Miyata scores between each amino acid substitution and its ancestral amino acid throughout the simulations.

For both the Base and Complex cases, the distributions of Miyata scores per amino acid from the Conflict and Buffering models were most distinguishable from each other in the strongest selection scenario at $N_e|s| = 100$. Here, the interquartile ranges of Miyata score distributions of the two models were completely separated at the end of simulations (fig6A, 6B; row 1), but they were basically indistinguishable from each other throughout the simulations when the selection is the weakest at $N_e|s| = 1$ (fig6A, 6B; row 3).

For $N_e|s| = 10$, the distributions of Miyata scores overlap more in the Base case compared with the Complex case (fig6A, 6B; row 2) because the positively selected mutations had a higher concentration of Miyata scores between 1 and 3 in the Complex case, which made the differences between Miyata scores more prominent. The same results can be observed in the strongest selection simulations, where the distance between interquartile ranges was also larger in the Complex cases than in the Base cases.

In summary, we are better able to distinguish between the Conflict and Buffering models using Miyata score distributions when there is strong selection, and when there is a more complicated parameterization of selection scheme as in the Complex models. Different infection/absence phase lengths did not have a large impact on the average Miyata scores across the simulations.

Comparison with the empirical data

To evaluate which model in our analysis better captures *bam's* observed patterns of sequence evolution within and between natural populations of *Drosophila*, we first performed our MK test on a population sample (n=89) of *D. melanogaster* (Lack et al. 2015), using divergence to the predicted common ancestral sequence with *D. simulans* as the outgroup and a randomly sampled sequence as the reference sequence used in the iMKT estimate. Analysis of these data reject neutrality in the direction of positive selection using the MK test with a p = 0.00015 and α estimated to be 0.91 (FWW correction, SNPs > 5% only). We used the number of nonsynonymous substitutions per nonsynonymous site (dN) calculated from iMKT results as the summary statistic to tune selection parameters of the two simulation models with only one *Wolbachia* infection-loss cycle.

While examining polymorphism levels would seem important to distinguish between Conflict and Buffering models, these levels are very sensitive to the length of *Wolbachia* infection and absence as we have modeled it, for example, due to the strong purifying selection occurring in the Conflict model when *Wolbachia* is lost. Thus, determining the time point for sampling is problematic for the empirical data as we do not know for a species that is infected with *Wolbachia* how long it has been infected, nor do we know for uninfected species when the last time they were infected (or even if they were). The problematic effect of this timing choice on P_n and P_s can be seen in Figures 3 and 4. As D_n is less sensitive to the sampling time points and represents the number of amino acid changes in *bam*, we chose to only use this parameter to evaluate how well our models fit to empirical data.

Applying our custom iMKT script to our empirical sequence data, we found that iMKT $D_n = 34$ and dN = 0.033 for the empirical *D. melanogaster* population. We initially found that Conflict models always predicted a much higher D_n than the empirical observation, while Buffering models often exhibited a much lower D_n. Such results showed the initially assumed ratio of codons under selection (RS=15%) and ratio of codons under constraints (RC=75%) could not reproduce similar results for the evolution of amino acids for either model. Thus, we chose to tune these two ratios of selected and constrained codons (RS and RC) under different strengths of positive selection ($N_e|s| = 100, 10, 1$) and explore under which parameter settings could we fit the empirical dN in each of our proposed models. When we achieved a matching dN, we then compared the Miyata scores per amino acid change in the observed data and our

simulation results and see whether a Conflict or a Buffering model is more similar to our observations.

For each selection coefficient *s*, we first ran simulations using RS and RC both sampled from a uniformly distributed grid of nine points ranging from 0 to 0.8, since the maximum proportion of conserved codons is 0.85, and assessed the resulting dN. Preliminary simulations revealed that for the Conflict models, dN was consistently more than two-fold overestimated for any proportion of selected sites greater than 0 (e.g., RS > 0, data not shown). Therefore, we refined the Conflict model grid search for RS to a uniform grid of 6 points from [0, 0.1], while keeping the full grid range for RC. For the Buffering models, we kept the full range of the RS grid as we did find parameters that fit the observed dN. For each pair of parameters for all models, we ran 50 simulations and calculated the mean of dN ($d\bar{N}$) across the runs. We then compared the difference between the empirical dN and $d\bar{N}$. The best pair of RS and RC was the one that led to the smallest difference between $d\bar{N}$ and the empirical dN under each selection coefficient *s*.

For the models with selection coefficient $N_e|s| = 1$, all combinations of the two ratios reproduced similar results consistent with effective neutrality (fig 7). For moderate or strong selection, the best-fit parameters are shown in Table 2.

Analyses of Conflict and Buffering Models Best Fitting the Empirical Data

To evaluate how well the Conflict and Buffering models implemented with the best-fit pairs of RS and RC recapitulate the empirical data for *D. melanogaster*, we performed the same iMKT analysis and Miyata score analysis for the resulting simulations. Positive true α's were observed in the Conflict Base, Buffering Base and Conflict Complex models across different phase lengths, indicating that positive selection was present under these scenarios. However, iMKT could only identify positive selection by α and statistically significant p-values in the two Conflict models with strong selection at $N_e|s| = 100$. Moderate selection at $N_e|s| = 10$ in the Conflict models or any levels of selection in the two Buffering models was not detected by iMKT p-values or inferred α (fig. 8).

In addition, we calculated the empirical per-site Miyata scores between the current *D. melanogaster* sequences and their predicted common ancestral sequence shared with *D. simulans* (supplemental file S2), and compared it with the distributions of per-site Miyata scores simulated

from the best-fitted RS and RC at different timepoints. The end of the simulations at 45,000 scaled generations represents the actual divergence time between the ancestral sequence and the extant *D. melanogaster* and *D. simulans* species. At this time point, the interquartile ranges of Miyata scores of the Conflict and Buffering models have separated from each other, with fully non-overlapping interquartile distributions in the Complex models. In all models, the per-site Miyata score of *D. melanogaster* are located closer to the center of the distributions from the Buffering models than to the center of distributions from the Conflict models (Figure 9).

In summary, the best-fit Conflict models with strong selection reproduced the most significant iMKT p-values and high estimates of α like that observed in the *D. melanogaster* sample, but the Miyata-score analysis indicated the Buffering models as a better fit for the evolution of the amino acids' biochemical properties. It is important to note that while the average iMKT α is extremely close to zero for all Buffering models, the lower whiskers on the box plots in fig 8B and 8C show that high iMKT inferred α's can, although infrequently, occur under the Buffering models as well.

Discussion

The increasing availability of DNA sequence datasets for diverse genes, genomes and organisms has led experimentalists to scan genes and genomes for footprints of natural selection. Using tests like the MK test, a striking number of cases of departures from neutrality have been revealed (e.g., Eyre-Walker 2006). In some cases, statistical evidence of strong positive selection can be easily associated with a proposed causal factor (e.g., genes involved in antiviral immunity or in mating behavior; e.g., McLaughlin and Malik 2017). In other cases, the driving factor is less clear.

In this study, we proposed two different models, the Conflict model and the Buffering model, to investigate different types of driving forces behind the signatures of positive selection at *bam*, motivated by its biological interactions with *Wolbachia*. The Conflict model is based on an arms race dynamics previously proposed to model the interactions between competing symbiotic species, which positively selected diversified amino acids. The alternative Buffering model we newly propose in this paper is based on another possible interaction between *bam* and *Wolbachia*, in which *Wolbachia* protects *bam* from the effects of deleterious mutations that can therefore accumulate during the *Wolbachia* infection phase by drift (equivalent to the relaxation

of functional constraints for amino acid mutations). When *Wolbachia* is lost, the constraints are reimposed and amino acids similar to *bam*'s ancestral state are selected for.

We used simulations to study the evolutionary process involved in each model and found that both models can generate positive selection as measured by the true α. A positive true α in the Conflict Base and Complex models aligns with our expectations of the represented interaction. More interestingly, the positive true α in the Buffering models reveals that *Wolbachia* need not function as a reproductive parasite in conflict with *bam* to drive positive selection in the host gene.

However, we must highlight the difference in the Buffering model's ability to generate positive selection and our ability to detect it. We found that in all simulations, the iMKT α generally underestimated the true α. This underestimation had a minimal effect on our interpretation of evolution in the Conflict models, as the true α was very large in all simulations outside of those with the weakest selection ($N_e|s| = 1$). On the other hand, with a maximum true α (~ 0.25) in the Buffering models' simulations, an underestimation led to a weak or absent signal of positive selection detectable by iMKT, which could further be confounded by statistical noise. Such findings highlight some limitations of the MK test that are consistent with the findings of others (Akashi 1999, Fay et al. 2001, Eyre-Walker and Keightley 2009, Zhai et al. 2009, Messer and Petrov 2013). Nevertheless, even with these limitations, the iMKT could still infer high α's, representing detection of positive selection, in some simulation runs under the Buffering models.

The Buffering models require the fixation of *Wolbachia*-buffered deleterious nonsynonymous mutations by drift for there to be resulting positive selection during a subsequent phase without *Wolbachia*. This effect is seen across the three different infection lengths that we simulated in the Buffering Base model. Thus, longer *Wolbachia* infection phases will increase the chance of detecting positive selection in a subsequent *Wolbachia* absence phase, though never to the level resulting from Conflict models. The average length of *Wolbachia* infection time is unknown for *Drosophila*, but a few studies have documented the minimum length of current *Wolbachia* infections. These include two independent studies that found the *w*Mel *Wolbachia* variant to have been in *D. melanogaster* for 79,000 and 80,000 *Drosophila* generations thus far (Richardson et al. 2012; Choi and Aquadro, 2014). These time periods are shorter than what we have simulated, but there is evidence to suggest turnover of *Wolbachia*

variants that could act as a longer standing infection period than currently documented (Riegler et al. 2005, Kriesner et al. 2013). Thus, *Wolbachia* infection of the length we have simulated, and with it a potential for subsequent positive selection, is not out of question.

In addition to phase lengths affecting the Buffering model results, population size could also play a large role. Because drift during the *Wolbachia* infection phase is what allows the buffered deleterious nonsynonymous mutations to fix, this model will likely lead to stronger signatures of positive selection for species with smaller N_e than this large population size *Drosophila* species since the time to fixation of neutral mutations is approximately $4N_e$ generations (Kimura and Ohta 1969).

To better evaluate the fit of the observed data from *D. melanogaster* to the predictions of the Conflict and Buffering models, we tuned the simulation selection parameters of both models to fit the observed nonsynonymous sequence divergence per nonsynonymous site (dN) between *D. melanogaster* and the inferred common ancestor with *D. simulans*. Explorative simulations are reflected in the empirically tuned simulations. Only the tuned Conflict model recapitulated the statistically significant positive iMKT α's that we observed for the *D. melanogaster* population. As in the general Buffering results discussed above, the tuned Buffering model can result in evidence of positive selection as indicated by a true α under certain conditions, but we can rarely detect it with the iMKT in *bam* with statistical significance. Interestingly, for the Miyata score analysis, we found that the Buffering models better fit our empirical data, as the Conflict models predicts greater amino acid diversity (assessed by the Miyata score) than we observe. Thus, combining these two results, we suggest that the Buffering model is a possible explanation behind the observed evolution in the *D. melanogaster bam* gene on the rare occasion that the iMKT is significant in the direction of positive selection. Nevertheless, a p-value less than or equal to 0.05 for the empirical MKT result is the typical criteria used by experimentalists to infer a departure from an equilibrium neutral model. Thus, with the current assumptions of our models, the Conflict model of an arms race between *Wolbachia* and *bam* is the better explanation for the signature of selection that we observe at *bam.*

We note that the best fit results for all models come with parameterizations that include a considerable proportion of neutral sites. This suggests that our model is missing important subtleties behind the evolution of *bam*. For instance, we have only used fixed selection coefficients throughout our simulations to model the selection coefficients for both beneficial

and deleterious mutations, while they could actually be drawn from some distribution. The cutoffs of Miyata scores to determine the characteristics of each mutation were also fixed and thus could also involve more customization based on the properties and functions of actual amino acids as well. It is also possible that a mixture of Conflict and Buffering models may be operating, with each driving evolution at a subset of sites. Importantly, while the underlying simplified assumptions as implemented in our models give them only a limited ability to capture the full details of the evolutionary processes, our simulations do demonstrate that the Conflict models have enough power to generate statistically significant signatures of positive selection at *bam*.

With regard to resolving the evolutionary interactions between *bam* and *Wolbachia* in *Drosophila*, it will now be important to explore other experimental evidence with respect to potential conflict, change in function or buffering. For example, we could test for evidence of positive selection in *Wolbachia* genes, as positive selection in *Wolbachia* is expected under the Conflict model where *Wolbachia* would co-evolve with *bam* to continue its impact on *Drosophila* fertility. There is already some evidence of positive selection at a few genes across different *Wolbachia* strains of arthropods and nematodes (Baldo et al. 2002; Baldo et al. 2010) but a much more thorough analysis of closely related *Wolbachia* strains infecting *D. melanogaster* is needed. To test for a conflict-like interaction between germline stem cell genes and *Wolbachia*, signals of selection in *Wolbachia* need to be examined solely within the *Drosophila* genus, since *Wolbachia* has a very different relationship with its nematode hosts (Taylor et al. 2005).

While our modeling study was motivated by the bursts of positive selection at *bam* and *Sxl* in *Drosophila* and the experimental interactions between *Wolbachia* and hypomorphs at these genes, both the Conflict model and the Buffering model should be investigated when we try to understand the signals of positive selection at other genes in *Drosophila*. Considering that *Wolbachia* infects some 50% or more of all arthropods (Hilgenboecker et al. 2008; Zug et al. 2012; Weinert et al. 2015), this means that there are potentially many yet undiscovered cases of strong episodic positive selection in other species. Genes of a greater length than *bam* are of particular interest as there is potentially more statistical power to detect positive selection resulting from the Buffering model.

We also want to emphasize that a fit to the Conflict compared to the Buffering model does not by itself imply a conflict drives the positive selection observed. A change in function that favors diversification of the protein-coding gene would also give similar results because, like the Conflict model, selection to refine a new function would likely favor positive selection for physicochemically different amino acids, which is selection for increasingly diverse Miyata scores. A recent analysis of CRISPR/Cas-9 generated nulls in five *Drosophila* species raises this possibility for *bam* (Bubnell et al. 2021). Whether the observed changes in function are associated with conflict with *Wolbachia* remains an open question as the two are not mutually exclusive.

Ultimately, we suggest that the Buffering model is a new entry to the suite of models that need to be considered in cases where molecular population genetic evidence is found for departures from selective neutrality consistent with positive selection. The Buffering model is a framework that could apply to populations that experience cycles of higher mutational loads, followed by positive selection. This is observed in seasonally small populations, where a drop in population size allows the fixation of some deleterious alleles that are subsequently purged from the population. Additionally, populations in changing environments may experience higher mutational loads at the onset of the change. This phenomenon would be similar to that of antagonistic pleiotropy, in which, for our case, one environment is more tolerant of various alleles, allowing some alleles to fix that would be considered deleterious in the subsequent environment. In the subsequent environment, positive selection favors new mutations that return the gene to its optimum sequence (Chen and Zhang 2020).

Supplemental Materials:

Supplemental materials are available at *Molecular Biology and Evolution online*.

Acknowledgements

This work was supported by the National Institute of General Medical Sciences at the National Institutes of Health grant number R01GM095793 to C.F.A. We thank Jesús Murga Moreno, Antoni Barbadilla Prados, and Sònia Casillas Viladerrams for discussing and sharing their iMKT script. We also thank Benjamin C. Haller for constructive discussion on implementing our

models in SLiM and feedback to improve the clarity of this manuscript and Jeffrey D. Jensen and Andrew G. Clark for thoughtful suggestions on an earlier draft of the manuscript.

Author Contributions

RS - coding, investigation, analysis, and writing. MW – conceptualization, investigation, analysis, and writing. PWM – writing and supervision. CFA - conceptualization, funding acquisition, and writing and supervision.

Data Availability

No new sequencing data were generated in this work; the employed data sets are listed throughout the text. Sequence alignments used are available as supplementary file S2, Supplementary material online. SLiM3 and python code for analyses used in this study are available online at github.com/runxi-shen/Modeling-Evolution-at-bam.

675 **References**

676

677 Akashi H. 1999. Inferring the fitness effects of DNA mutations from polymorphism and
678 divergence data: statistical power to detect directional selection under stationarity and free
679 recombination. *Genetics* 151:221-238.
680 Baldo L, Bartos JD, Werren JH, Bazzocchi C, Casiraghi M, Panelli S. 2002. Different rates of
681 nucleotide substitutions in Wolbachia endosymbionts of arthropods and nematodes: arms race or
682 host shifts? *Parassitologia* 44:179-187.
683 Baldo L, Desjardins CA, Russell JA, Stahlhut JK, Werren JH. 2010. Accelerated microevolution
684 in an outer membrane protein (OMP) of the intracellular bacteria Wolbachia. *BMC Evol Biol*.
685 10:48.
686 Bauer DuMont VL, Flores HA, Wright MH, Aquadro CF. 2007. Recurrent positive selection at
687 Bgcn, a key determinant of germ line differentiation, does not appear to be driven by simple
688 coevolution with its partner protein bam. *Mol Biol Evol.* 24:182-191.
689 Bauer DuMont VL, White SL, Zinshteyn D, Aquadro CF. 2021. Molecular population genetics
690 of Sex-lethal (Sxl) in the Drosophila melanogaster species group: a locus that genetically
691 interacts with Wolbachia pipientis in Drosophila melanogaster. *G3(Bethesda)* 11(8):jkab197.
692 Bubnell JE, Fernandez-Begne P, Ulbing CKS, Aquadro CF. 2021. Diverse wMel variants of
693 Wolbachia pipientis differentially rescue fertility and cytological defects of the bag of marbles
694 partial loss of function mutation in Drosophila melanogaster. *G3 (Bethesda)* 11(12): jkab312.
695 Campos JL, Zhao L, Charlesworth B. 2017. Estimating the parameters of background selection
696 and selective sweeps in Drosophila in the presence of gene conversion. *Proc Natl Acad Sci U S*
697 *A.* 114(24):E4762-E4771.
698 Charron C, Nicolaï M, Gallois JL, Robaglia C, Moury B, Palloix A, Caranta C. 2008. Natural
699 variation and functional analyses provide evidence for co-evolution between plant eIF4E and
700 potyviral VPg. *Plant J* 54:56-68.
701 Chen P, Zhang J. 2020. Antagonistic pleiotropy conceals molecular adaptations in changing
702 environments. *Nat Ecol Evol*. 4:461-469.
703 Choi, J. Y., and Aquadro, C. F. 2014. The coevolutionary period of Wolbachia pipientis infecting
704 Drosophila ananassae and its impact on the evolution of the host germline stem cell regulating
705 genes. *Mol Biol and Evol*, *31*(9), 2457–2471.

706 Comeron JM, Ratnappan R, Bailin S. 2012. The Many Landscapes of Recombination in
707 Drosophila melanogaster. *PLOS Genetics* 8:33-35.
708 Demogines A, Abraham J, Choe H, Farzan M, Sawyer SL. 2013. Dual Host-Virus Arms Races
709 Shape an Essential Housekeeping Protein. *PLOS Biology* 11:e1001571.
710 Eyre-Walker A. 2006. The genomic rate of adaptive evolution. *Trends Ecol Evol*. 21(10): 569-
711 575.
712 Eyre-Walker A and Keightley PD. 2009. Estimating the rate of adaptive molecular evolution of
713 slightly deleterious mutations and population size change. *Mol Biol and Evol*. 26:2097-2108.
714 Fay JC, Wyckoff GJ, Wu C-I. 2001. Positive and Negative Selection on the Human Genome.
715 *Genetics* 158:1227.
716 Flores HA, Bauer DuMont VLB, Fatoo A, Hubbard D, Hijji M, Barbash DA, Aquadro CF.
717 2015a. Adaptive evolution of genes involved in the regulation of germline stem cells in
718 Drosophila melanogaster and D. simulans. *G3 (Bethesda)* 5(4):583-592.
719 Flores HA, Bubnell JE, Aquadro CF, Barbash DA. 2015b. The Drosophila bag of marbles Gene
720 Interacts Genetically with Wolbachia and Shows Female-Specific Effects of Divergence. *PLOS*
721 *Genetics* 11:1-31.
722 Grantham R. 1974. Amino acid difference formula to help explain protein evolution. *Science*
723 185:862-864.
724 Haller BC and Messer PW. 2019. SLiM 3: Forward genetic simulations beyond the Wright-
725 Fisher model. *Mol Biol and Evol*. 36(3):632-637.
726 Haller BC, Galloway J, Kelleher J, Messer PW, Ralph PL. 2019. Tree-sequence recording in
727 SLiM opens new horizons for forward-time simulation of whole genomes. *Mol Ecol Resour.*
728 19(2):552-566.
729 Henikoff S, Henikoff JG. 1992. Amino acid substitution matrices from protein blocks. *Proc Natl*
730 *Acad Sci U S A* 89:10915-10919.
731 Hilgenboecker K, Hammerstein P, Schlattmann P, Telschow A, Werren JH. 2008. How many
732 species are infected with Wolbachia?--A statistical analysis of current data. *FEMS Microbiol Lett*
733 281:215-220.
734 Keightley PD, Ness RW, Halligan DL, Haddrill PR. 2014. Estimation of the spontaneous
735 mutation rate per nucleotide site in a Drosophila melanogaster full-sib family. *Genetics* 196:313-
736 320.

737 Keightley PD, Trivedi U, Thomson M, Oliver F, Kumar S, Blaxter ML. 2009. Analysis of the
738 genome sequences of three Drosophila melanogaster spontaneous mutation accumulation lines.
739 Genome Res. 19:1195-1201.
740 Kimura M, Ohta T. 1969. The average number of generations until fixation of a mutant gene in a
741 finite population. *Genetics* 61:763-771.
742 Kriesner P, Hoffman AA, Lee SF, Turelli M, Weeks AR. 2013. Rapid sequential spread of two
743 Wolbachia variants in Drosophila simulans. *PLoS Pathog* 9(9): e1003607.
744 Lack JB, Cardeno CM, Crepeau MW, Taylor W, Corbett-Detig RB, Stevens KA, Langley CH,
745 Pool JE. 2015. The Drosophila genome nexus: A population genomic resource of 623 Drosophila
746 melanogaster genomes, including 197 from a single ancestral range population. *Genetics*
747 199:1229-1241.
748 Löytynoja A. 2014. Phylogeny-aware alignment with PRANK. *Methods Mol Biol*. 1079:155-
749 170.
750 McDonald JH, Kreitman M. 1991. Adaptive protein evolution at the Adh locus in Drosophila.
751 *Nature* 351:652-654.
752 McLaughlin RN, Malik HS. 2017. Genetic conflicts: The usual suspects and beyond. *J Exp Biol*.
753 220:6-17.
754 Meany MK, Conner WR, Richter SV, Bailey JA, Turelli M, Cooper BS. 2019. Loss of
755 cytoplasmic incompatibility and minimal fecundity effects explain relatively low Wolbachia
756 frequencies in Drosophila mauritiana. *Evolution* 73:1278-1295.
757 Messer PW and Petrov DA. 2013. Frequent adaptation and the McDonald Kreitman test. *PNAS*
758 110:8615-8620.
759 Miyata T, Miyazawa S, Yasunaga T. 1979. Two types of amino acid substitutions in protein
760 evolution. *J Mol Evol*. 12:219-236.
761 Murga-Moreno J, Coronado-Zamora M, Hervas S, Casillas S, Barbadilla A. 2019. iMKT: The
762 integrative McDonald and Kreitman test. *Nucleic Acids Res* 47:W283-W288.
763 Richardson MF, Weinert LA, Welch JJ, Linheiro RS, Magwire MM, Jiggins FM, Bergman CM.
764 2012. Population genomics of the Wolbachia endosymbiont in Drosophila melanogaster. *PLOS*
765 *Genetics* 8:e1003129.
766 Riegler M, Sidhu M, Miller WJ, O'Neill SL. 2005. Evidence for a global Wolbachia replacement
767 in Drosophila melanogaster. *Curr Biol.* 15:1428-1433

768 Russo CA, Takezaki N, Nei M. 1995. Molecular phylogeny and divergence times of drosophilid
769 species. *Mol Biol and Evol*. 12:391-404.
770 Signor SA, New FN, Nuzhdin S. 2018. A Large Panel of Drosophila simulans Reveals an
771 Abundance of Common Variants. *Genome Biol and Evol*. 10:189-206.
772 Smith NGC, Eyre-Walker A. 2002. Adaptive protein evolution in Drosophila. *Nature* 415:1022-
773 1024.
774 Starr DJ, Cline TW. 2002. A host-parasite interaction rescues Drosophila oogenesis defects.
775 *Nature* 418:76-79.
776 Taylor MJ, Bandi C, Hoerauf A. 2005. Wolbachia bacterial endosymbionts of filarial nematodes.
777 *Adv Parasitol* 60:245-284.
778 Turelli M, Cooper BS, Richardson KM, Ginsberg PS, Peckenpaugh B, Antelope CX, Kim KJ,
779 May MR, Abrieux A, Wilson DA, et al. 2018. Rapid global spread of wRi-like Wolbachia across
780 multiple Drosophila. *Curr Biol*. 28:963-971.e968.
781 Weinert LA, Araujo-Jnr EV, Ahmed MZ, Welch JJ. 2015. The incidence of bacterial
782 endosymbionts in terrestrial arthropods. *Proc R Soc B Biol Sci*. 282:20150249.
783 Yang Z. 2007. PAML 4: Phylogenetic analysis by maximum likelihood. *Mol Biol and Evol*.
784 24:1586-1591.
785 Zhai W, Nielsen R, Slatkin M. 2009. An investigation of the statistical power of neutrality tests
786 based on comparative and population genetic data. *Mol Biol and Evol.* 26:273-283.
787 Zug R, Hammerstein P. 2012. Still a host of hosts for Wolbachia: Analysis of recent data
788 suggests that 40% of terrestrial arthropod species are infected. *PLoS One* 7:e38544.
789
790

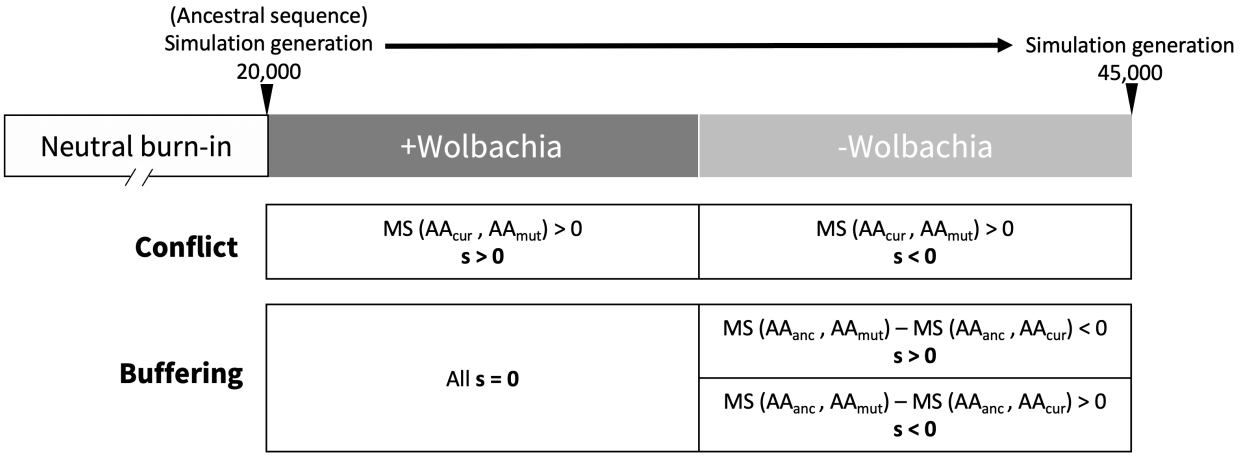

Fig. 1. Simulation setup for Conflict and Buffering Base models. Selection on new nonsynonymous mutations (mutated amino acid, AA_{mut}) is determined by their Miyata score (MS) to the appropriate reference amino acid (the current amino acid, AA_{cur}, or the ancestral amino acid, AA_{anc}).

797

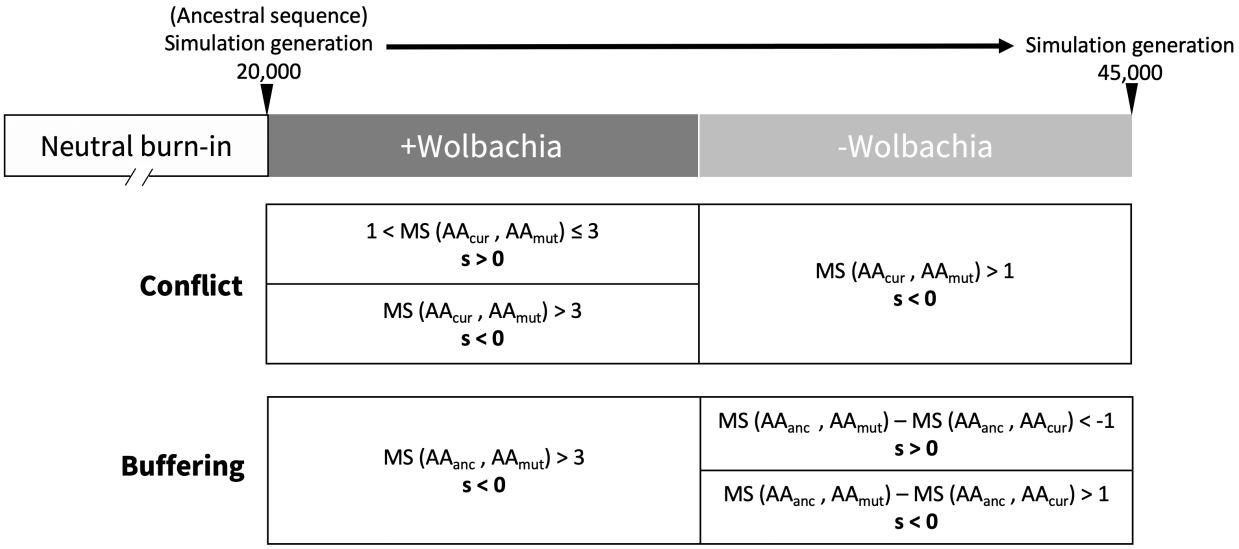

798

799 **Fig. 2. Simulation setup for Conflict and Buffering Complex models.** Selection on new
800 nonsynonymous mutations (mutated amino acid, AA_{mut}) is determined by their Miyata score
801 (MS) to the appropriate reference amino acid (the current amino acid, AA_{cur}, or the ancestral
802 amino acid, AA_{anc}).

803

804

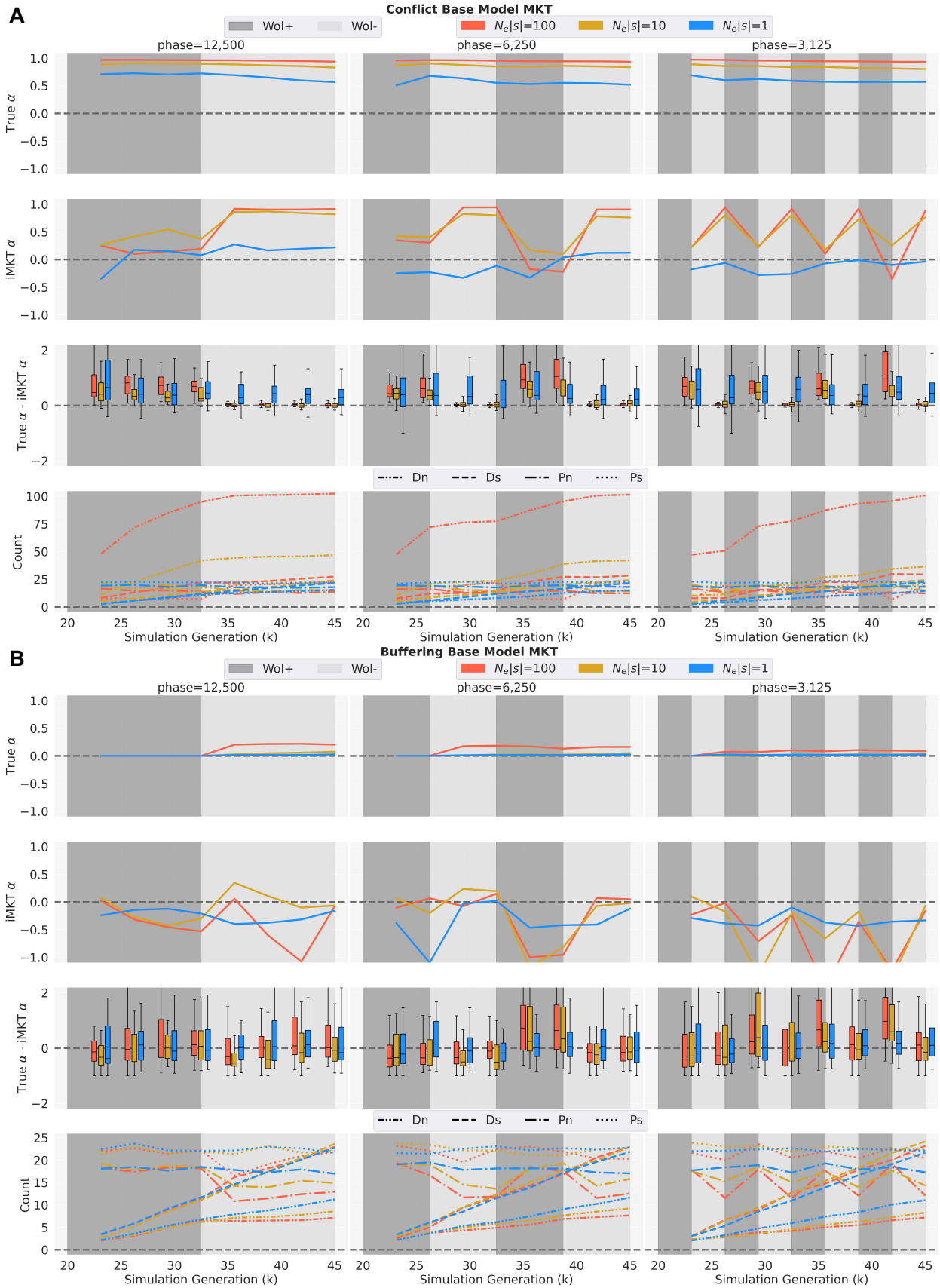

806 **Fig. 3. MK test results of simulations for two base models.** (A) Conflict model; (B) Buffering
807 model. Each panel shows MKT analyses with different selection coefficients of $N_e|s|$=100,
808 $N_e|s|$=10, and $N_e|s|$=1 graphed across alternating phases (phase length=12,500, 6,250, 3,125 and
809 simulation generations) of *Wolbachia* infection (Wol+, dark grey) and *Wolbachia* absence (Wol-,
810 light grey) post-burn-in period. In each panel, row 1: the average true α in the simulations; row
811 2: the average iMKT α in the simulations (FWW correction, SNPs frequency > 5% only); row 3:
812 the distributions of differences between the true and iMKT α every 3,125 simulation
813 generations; row 4: The average of each iMKT component (D_n, D_s, P_n, P_s).
814

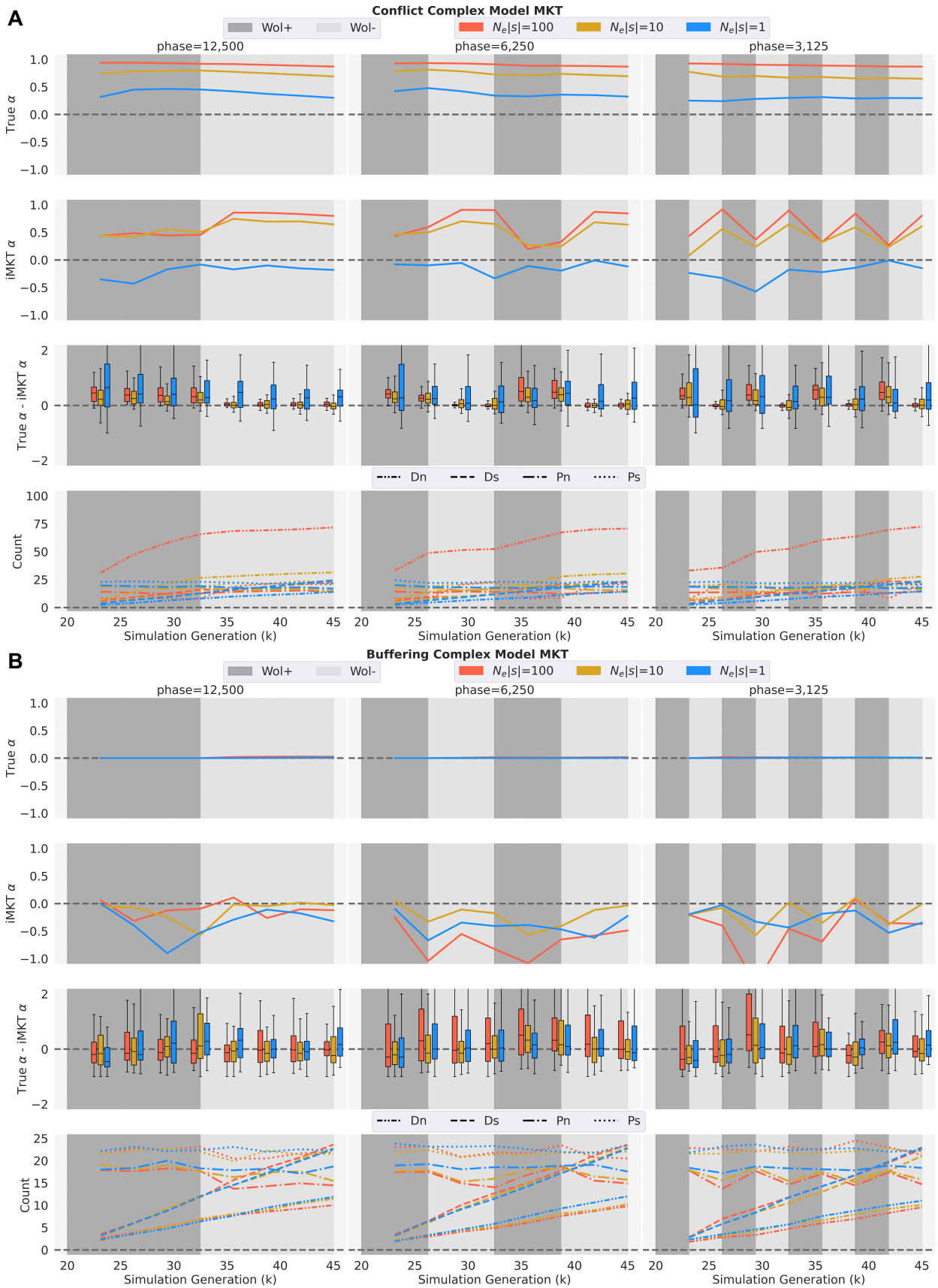

Fig. 4. MK test results of simulations for two complex models: (A) Conflict model, (B) Buffering model. Each panel shows MKT analyses with different selection coefficients of $N_e|s|$=100, $N_e|s|$=10, and $N_e|s|$=1 graphed across alternating phases (phase length=12,500, 6,250, 3,125 and simulation generations) of *Wolbachia* infection (Wol+, dark grey) and *Wolbachia* absence (Wol-, light grey) post-burn-in period. In each panel, row 1: the average true α in the simulations; row 2: the average iMKT α in the simulations (FWW correction, SNPs frequency > 5% only); row 3: the distributions of differences between the true and iMKT α every 3,125 simulation generations; row 4: The average of each iMKT component (D_n, D_s, P_n, P_s).

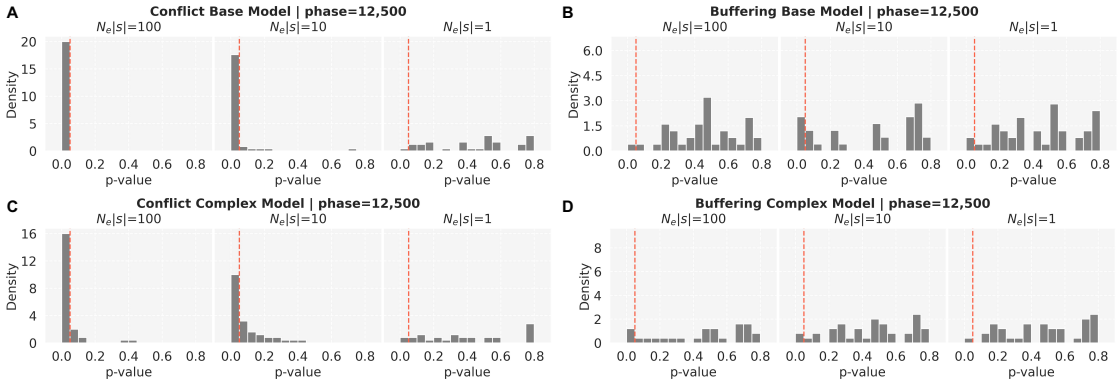

Fig. 5. Distributions of iMKT p-values. iMKT p-values (FWW correction, SNPs frequency > 5% only) for simulation runs with *Wolbachia* phase=12,500 simulation generations and $N_e|s|$=100, 10, 1 for the simulated models at 45,000 simulation generation. The vertical red line denotes p-value=0.05. Note that distributions are normalized to have an area of 1 under the histograms. (A) Conflict base model; (B) Buffering base model; (C) Conflict complex model; (D) Buffering complex model.

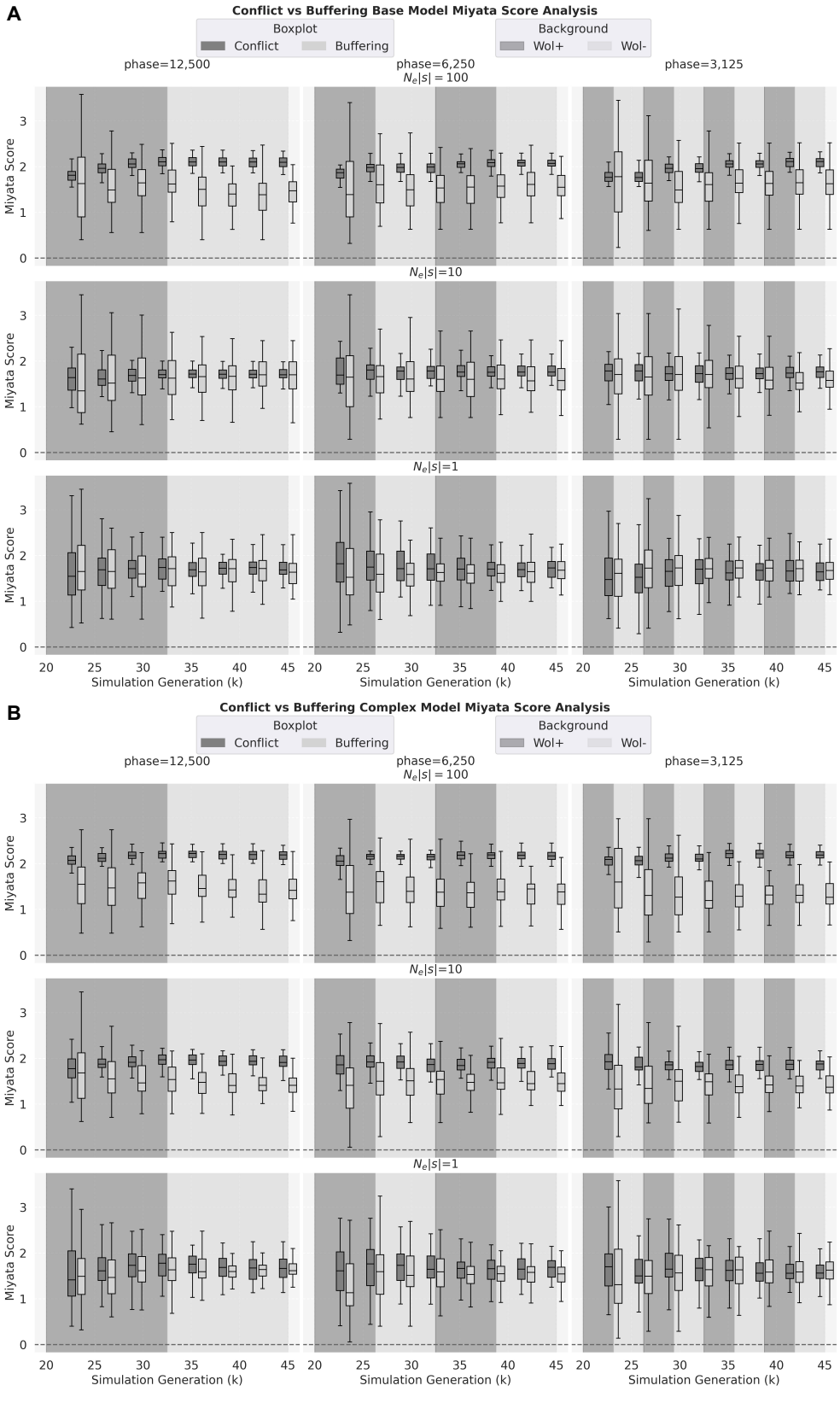

831

Fig. 6. The distribution of Miyata scores per amino acid substitution. Miyata scores per amino acid substitution across multiple runs for substitutions between the consensus sequence at the end of a given simulation generation and the ancestral sequence. Data is shown for both the Conflict model (dark grey) and Buffering model (light grey) at every 3,125 simulated generations post burn-in for different phase lengths.

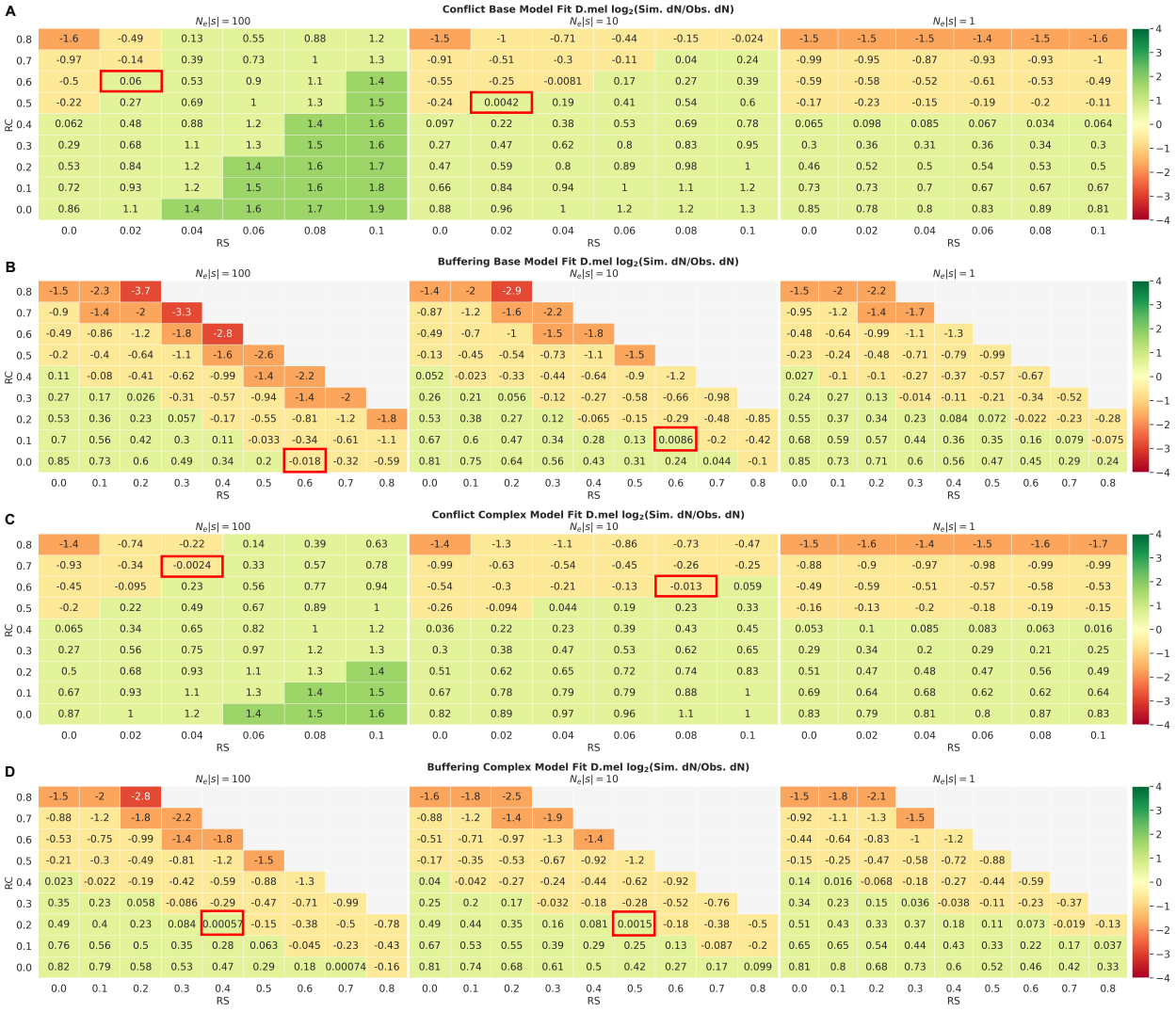

Fig. 7. Heatmap of $log_2 \frac{Simulation\ dN}{Observed\ dN}$ for four models to fit the empirical data. For each model, average dN was calculated across 50 simulation runs per each pair of conserved-site ratio and selection-site ratio to find the combination of parameters best fitting the empirical dN. Red boxes highlight the pairs of parameters used to investigate which model is preferred to recapitulate the observed data in iMKT and Miyata score analysis.

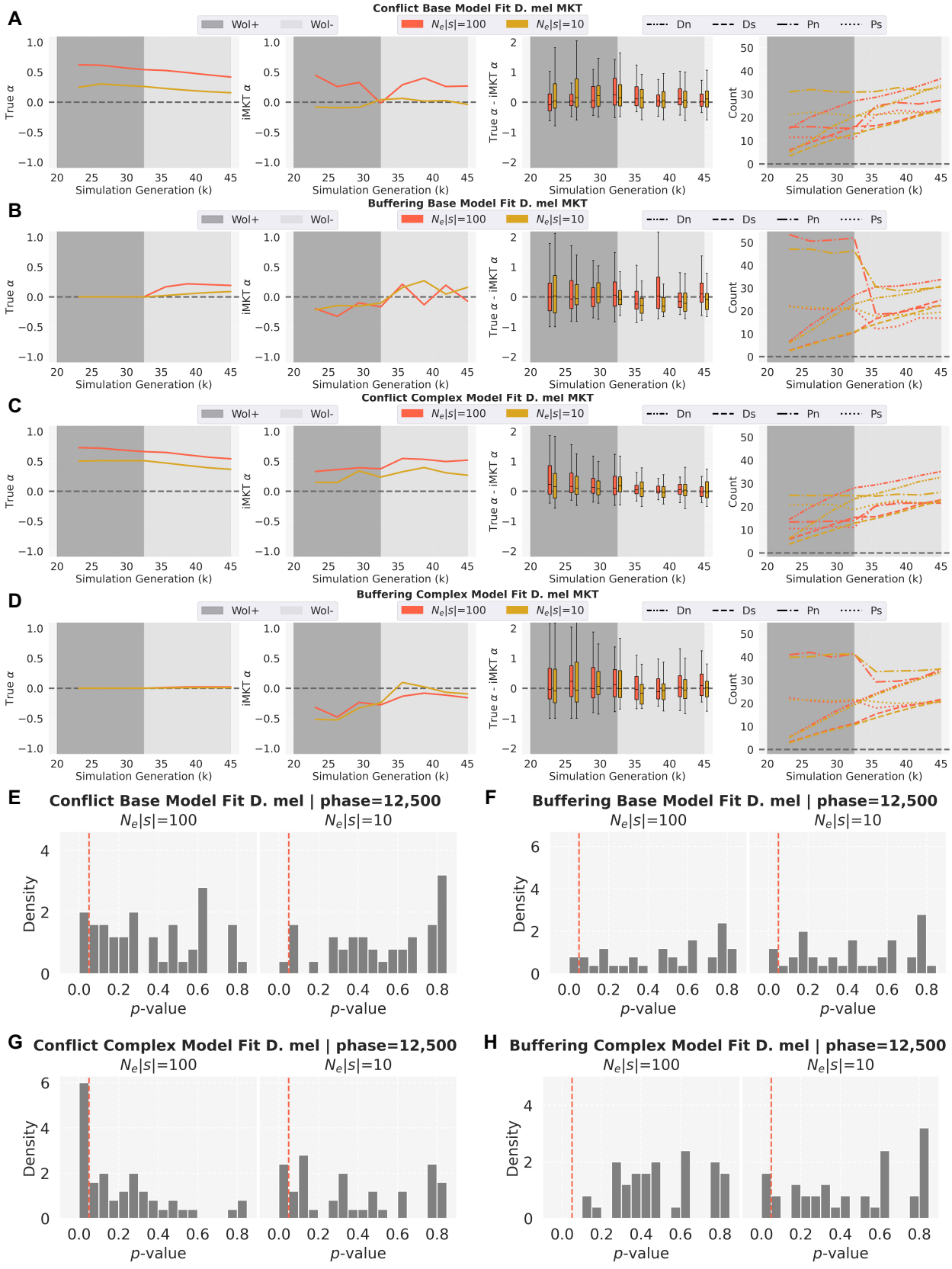

Fig. 8. MK test results of simulations for best-fit models for *D. melanogaster*. (A) MK test α analysis of each model with different selection coefficients of $N_e|s|$=100, $N_e|s|$=10 graphed at phase length=12,500 simulation generations of *Wolbachia* infection (Wol+, dark grey) and *Wolbachia* absence (Wol-, light grey) post-burn-in period. In each panel, row 1: the average true α in the simulations; row 2: the average iMKT α in the simulations (FWW correction, SNPs frequency > 5% only); row 3: the distributions of differences between the true and iMKT α every 3,125 simulation generations; row 4: The average of each iMKT component (D_n, D_s, P_n, P_s). (B) Distributions of iMKT p-values. iMKT p-values (FWW correction, SNPs frequency > 5% only) for simulation runs with *Wolbachia* phase=12,500 simulation generations and $N_e|s|$=100, 10 for the simulated models at 45,000 simulation generation. The vertical red line denotes p-value=0.05. Note that distributions are normalized to have an area of 1 under the histograms.

859

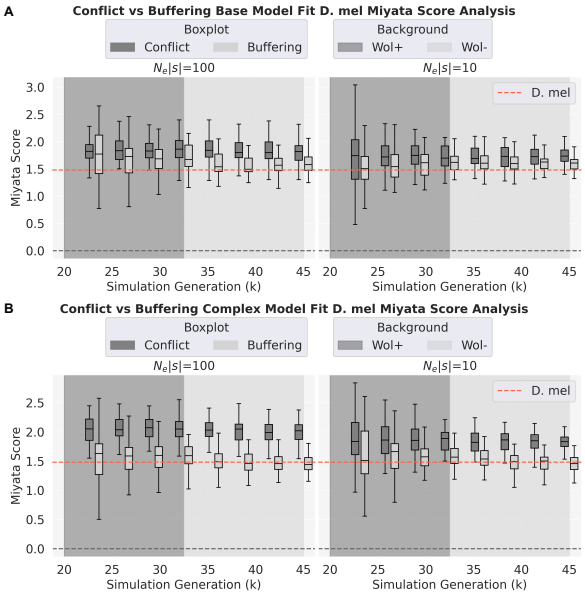

860

861 **Fig. 9. Distributions of Miyata score for the *D. melanogaster* samples from the simulations**
862 **with best-fit parameters.** The boxplots are the distributions of Miyata scores for each model at
863 every 3,125 generation. (A) Conflict and Base models; (B) Conflict and Buffering Complex
864 model. The distributions are compared with the observed summary statistics of *D. melanogaster*
865 empirical data (red horizontal line).

866 **Table 1.** Empirical (biological) estimates for evolutionary parameters and scaled estimates used
867 for simulation.

Parameter	N_e	ρ	μ	t
Empirical Estimate	1e6	1e-8	2.8e-9	2.5e7
Scaled Estimate (simulation)	1e3	1e-5	2.8e-6	2.5e4

868 N_e: effective population size; ρ: recombination rate; μ: mutation rate; t: time in unit of
869 generation
870

871 **Table 2.** Best fit RS and RC parameters for $N_e|s|$ =10 and 100 for Conflict and Buffering models.

	$N_e\|s\|$	RS	RC
Conflict	10	0.02	0.5
Base	100	0.02	0.6
Buffering	10	0.6	0.1
Base	100	0.6	0.0
Conflict	10	0.08	0.6
Complex	100	0.04	0.7
Buffering	10	0.2	0.5
Complex	100	0.4	0.2

872